

Magnetoelastic study on the frustrated quasi-one-dimensional spin- $\frac{1}{2}$ magnet LiCuVO₄A. Miyata,¹ T. Hikihara,² S. Furukawa,³ R. K. Kremer,⁴ S. Zherlitsyn,⁵ and J. Wosnitza^{1,5}¹*Hochfeld-Magnetlabor Dresden (HLD-EMFL) and Würzburg-Dresden Cluster of Excellence ct.qmat, Helmholtz-Zentrum Dresden-Rossendorf, 01328 Dresden, Germany*²*Faculty of Science and Technology, Gunma University, Kiryu, Gunma 376-8515, Japan*³*Department of Physics, Keio University, 3-14-1 Hiyoshi, Kohoku-ku, Yokohama, Kanagawa 223-8522, Japan*⁴*Max-Planck-Institut für Festkörperforschung, 70569 Stuttgart, Germany*⁵*Institut für Festkörper- und Materialphysik, TU Dresden, 01069 Dresden, Germany* (Received 16 October 2020; revised 14 December 2020; accepted 16 December 2020; published 8 January 2021)

We investigated the magnetoelastic properties of the quasi-one-dimensional spin- $\frac{1}{2}$ frustrated magnet LiCuVO₄. Longitudinal-magnetostriction experiments were performed at 1.5 K in high magnetic fields of up to 60 T applied along the b axis, i.e., the spin-chain direction. The magnetostriction data qualitatively resemble the magnetization results, and saturate at $H_{\text{sat}} \approx 54$ T, with a relative change in sample length of $\Delta L/L \approx 1.8 \times 10^{-4}$. Remarkably, both the magnetostriction and the magnetization evolve gradually between $H_{c3} \approx 48$ T and H_{sat} , indicating that the two quantities consistently detect the spin-nematic phase just below the saturation. Numerical analyses for a weakly coupled spin-chain model reveal that the observed magnetostriction can overall be understood within an exchange-contraction mechanism. Small deviations found may indicate nontrivial changes in local correlations associated with the field-induced phase transitions.

DOI: [10.1103/PhysRevB.103.014411](https://doi.org/10.1103/PhysRevB.103.014411)**I. INTRODUCTION**

One-dimensional (1D) quantum-spin magnets with competing interactions have been intensively studied for decades to search for unconventional quantum phases that result from the interplay between strong quantum fluctuations and magnetic frustration. As 1D systems generally allow a simpler theoretical treatment compared with higher-dimensional ones, they provide an ideal platform for studying quantum phases through a close comparison between experimental and theoretical approaches. One example is the spin-nematic phase, a magnetic analog of the nematic liquid-crystal phase, where the spin-rotational symmetry is spontaneously broken while translational and time-reversal symmetries are preserved. This new type of quantum phase has been discussed in a variety of 1D spin models, including spin- $\frac{1}{2}$ [1–4] and spin-1 [5,6] chains. In the spin- $\frac{1}{2}$ case, magnon bound states (bimagnons) arise from a competition between ferromagnetic nearest-neighbor $J_1 < 0$ and antiferromagnetic next-nearest-neighbor $J_2 > 0$ interactions, and play a crucial role in the formation of the spin-nematic phase. Upon condensation, bimagnons form a Tomonaga-Luttinger liquid (TLL), which shows dominant spin density wave (SDW) or nematic quasi-long-range correlations at low and high fields, respectively.

One well-studied spin-nematic candidate is the orthorhombic inverse spinel LiCuVO₄, where magnetic Cu²⁺ ions form spin- $\frac{1}{2}$ chains with two dominant exchange interactions, J_1 and J_2 , along the crystallographic b axis (Fig. 1) [7–10]. Weak interchain interactions (such as $J_5 < 0$) lead to a three-dimensional (3D) magnetic long-range order below $T_c \approx 2.3$ K with an incommensurate planar spiral structure lying

in the ab plane [11,12]. This spiral structure, which induces ferroelectricity through magnetoelectric coupling, has spurred additional interest in LiCuVO₄ in terms of multiferroicity [13–16].

When applying magnetic fields, a phase transition to an incommensurate collinear SDW phase takes place at $H_{c2} \approx 7.5$ T [17–19]. Such a SDW phase is expected to appear when the SDW correlations of a bimagnon TLL are stabilized by interchain interactions [20,21]. This picture has been corroborated by neutron-scattering [22], nuclear magnetic resonance (NMR) [23], and spin Seebeck effect [24] experiments. With further increasing magnetic field, the SDW correlations are weakened in favor of the nematic correlations, and as a result, a 3D nematic long-range order is stabilized just below the saturation field, as theoretically discussed in Refs. [20,21,25,26]. Remarkably, high-field magnetization [27], NMR [28], magnetocaloric effect (MCE), and ultrasound [29] measurements have reported evidence of this 3D spin-nematic state between H_{c3} and H_{sat} , which are about 40 and 45 T for the magnetic field applied along the c axis, and about 48 and 53 T along the a and b axes.

While a large number of experiments have been performed on LiCuVO₄, there have been only few studies on its magnetoelastic properties. Mourigal *et al.* have proposed that the magnetostriction is negligible in LiCuVO₄ based on specific-heat and neutron-scattering experiments, and that the multiferroicity arises from a purely electronic spin-supercurrent mechanism [15]. In contrast, recent thermal expansion and magnetostriction experiments in low magnetic fields of up to 9 T by Grams *et al.* revealed a sizable magnetoelastic coupling in LiCuVO₄ [30].

In this paper, we report longitudinal magnetostriction measurements of LiCuVO_4 at 1.5 K in high magnetic fields of up to 60 T applied along the b axis, i.e., the 1D spin-chain direction. The observed magnetostriction is as large as $\Delta L/L \approx 1.8 \times 10^{-4}$ at high fields, indicating that LiCuVO_4 has a sizable magnetoelastic coupling as reported previously [29,30]. The magnetostriction data qualitatively resemble the magnetization reported in Ref. [28]. In particular, both quantities evolve gradually between H_{c3} and H_{sat} , indicating that the magnetostriction can also probe the 3D spin-nematic state appearing just below the saturation. Furthermore, we analyze the magnetostriction data of LiCuVO_4 within an exchange-striction model with exchange interactions modified linearly by the distance between the involved spins. The density matrix renormalization group (DMRG) and exact diagonalization (ED) analyses for the J_1 - J_2 (- J_5) spin-chain model show an overall agreement with our experimental results. Small deviations found may indicate nontrivial changes in local correlations associated with field-induced phase transitions. A more refined treatment of the interchain coupling or introduction of additional interactions, such as a Dzyaloshinskii-Moriya (DM) term, is needed to explain the magnetoelastic properties of LiCuVO_4 in general detail.

II. METHODS

Longitudinal-magnetostriction measurements were performed by the optical fiber Bragg grating (FBG) method [31] in pulsed magnetic fields of up to 60 T with a whole pulse duration of 25 ms at the HLD-EMFL in Dresden. The relative length change $\Delta L/L$ was obtained from the Bragg wavelength shift of the FBG. A high-quality LiCuVO_4 single crystal with a size of $1.9 \times 2.0 \times 0.65 \text{ mm}^3$ was used in this study, which is the same one previously used in the magnetocaloric effect and ultrasound experiments by Gen *et al.* [29]. Magnetic field was applied along the orthorhombic b axis, which is the spin-chain direction ($\mathbf{H} \parallel \Delta L/L \parallel b$ axis). Note that the magnetic field was applied along the c axis in Ref. [29].

Numerical analyses were conducted for the J_1 - J_2 - J_5 model that describes magnetic interactions in the ab plane [Fig. 1(b)]. We use the ratio $J_1 : J_2 : J_5 = -0.42 : 1 : -0.11$ as obtained from neutron-scattering experiments reported in Ref. [9]. For the Landé g -factor, we take the value $g = 2.095$ along the b axis from Ref. [32]. We then set $J_2 = 4.0 \text{ meV}$ so that

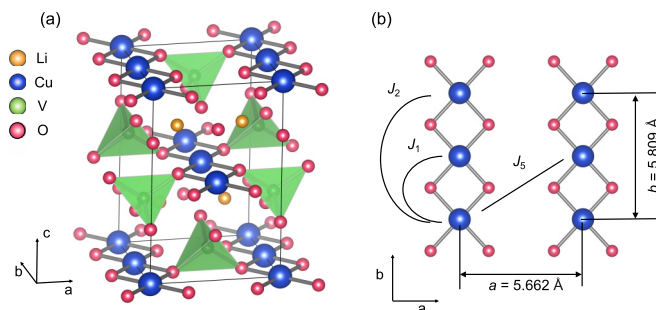


FIG. 1. (a) Crystal structure of LiCuVO_4 (b) Two Cu_2O chains exist in the ab plane with three main exchange interactions J_1 , J_2 , and J_5 . The lattice constants a and b are 5.662 and 5.809 Å, respectively [7].

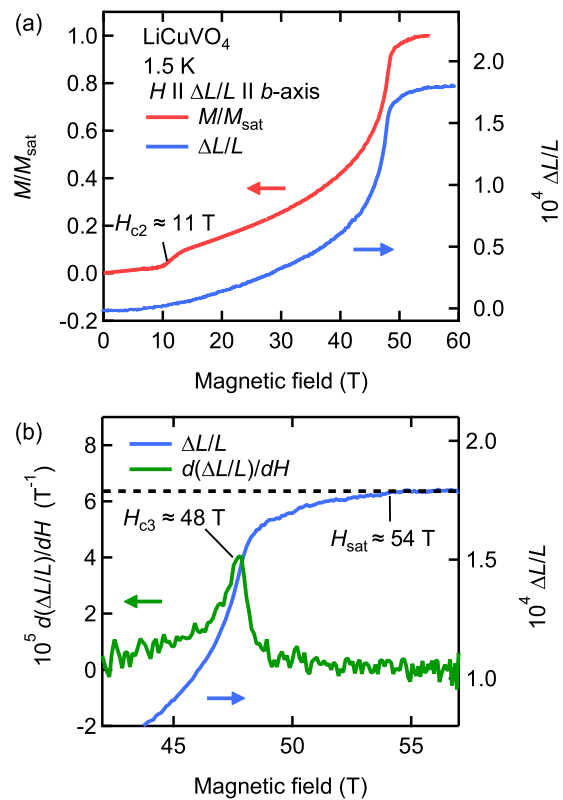


FIG. 2. (a) Longitudinal magnetostriction $\Delta L/L$ of LiCuVO_4 and the normalized magnetization M/M_{sat} from Ref. [28] as a function of magnetic field ($\mathbf{H} \parallel \Delta L/L \parallel b$ axis). (b) Longitudinal magnetostriction $\Delta L/L$ of LiCuVO_4 and its derivative in the vicinity of the saturation field. The critical fields H_{c2} , H_{c3} , and H_{sat} are estimated as 11, 48, and 54 T, respectively.

the theoretical saturation field is adjusted to 48 T, at which the experimental magnetization curve is the steepest; see Appendix B. This value is quite close to $J_2 = 3.8 \text{ meV}$ reported in Ref. [9]. DMRG calculations were performed for the pure 1D J_1 - J_2 model with up to 168 spins. We computed the lowest-energy state in each subspace characterized by the magnetization M and obtained the ground-state energy and local correlation functions as functions of M (see Appendix A for details). The effects of the interchain coupling J_5 on the ground-state energy were taken into account in a mean-field manner following Ref. [33]. As a complementary analysis, ED calculations based on TITPACK version 2 [34] were performed directly for the J_1 - J_2 - J_5 model with up to 28 spins on the 2D plane. Both the DMRG and ED results show an overall agreement with the experimental magnetization, as shown in Appendix B.

III. RESULTS AND DISCUSSION

A. Magnetostriction measurements and exchange-striction mechanism

Figure 2(a) shows the longitudinal magnetostriction $\Delta L/L$ of LiCuVO_4 in magnetic fields of up to 60 T ($\mathbf{H} \parallel \Delta L/L \parallel b$ axis) with the normalized magnetization M/M_{sat} taken from Ref. [28]. Note that the LiCuVO_4 sample used in

magnetization measurements was from the same batch as that used in the present magnetostriction study. The magnetostriction data qualitatively resemble the magnetization up to the saturation, except that no transition was detected at around 11 T (labeled as H_{c2} in the magnetization). A spiral-plane flop transition has been reported at $H_{c1} \approx 3$ T [27], which is not observed in the pulsed-field magnetization and magnetostriction experiments. At saturation, the observed magnetostriction is as large as $\Delta L/L \approx 1.8 \times 10^{-4}$, indicating a sizable magnetoelastic coupling in LiCuVO₄ as also reported recently [29,30].

To highlight the anomaly in high magnetic fields, the derivative of the longitudinal magnetostriction $d(\Delta L/L)/dH$ is shown in Fig. 2(b). Notably, the magnetostriction still grows above 48 T (H_{c3}), at which a clear peak in $d(\Delta L/L)/dH$ is observed, and it saturates around 54 T (H_{sat}). Similar behavior has also been observed in magnetization and NMR experiments, as reported previously in Refs. [27,28]; in these works, evidence for the existence of a 3D spin-nematic phase between H_{c3} and H_{sat} was given. The observed similarity indicates that the magnetostriction can consistently detect the 3D spin-nematic phase as well.

To understand the microscopic origin of the magnetostriction, we adopt the following exchange-striction model for a 1D frustrated J_1 - J_2 spin-chain system [35,36],

$$\mathcal{H}_{es} = \sum_{n=1,2} \sum_j (J_n - f_n \epsilon) \mathbf{S}_j \cdot \mathbf{S}_{j+n} + \frac{N_{ID} k'}{2} \epsilon^2 - g \mu_B H \sum_j S_j^z, \quad (1)$$

where $\epsilon = \Delta L/L$, f_n is the magnetoelastic coupling coefficient, k' is the elastic constant per Cu²⁺ ion, and N_{ID} is the number of Cu²⁺ ions in the chain. For a fixed field H or a fixed magnetization M , the equilibrium value of ϵ can be determined from minimizing the expectation value of \mathcal{H}_{es} over ϵ . To compare with the experimental data, we set ϵ to zero for $M = 0$, obtaining

$$\epsilon(M) = \frac{1}{k'} \sum_{n=1,2} f_n (\langle \mathbf{S}_j \cdot \mathbf{S}_{j+n} \rangle_M - \langle \mathbf{S}_j \cdot \mathbf{S}_{j+n} \rangle_{M=0}), \quad (2)$$

where $\langle \dots \rangle_M$ denotes the expectation value at the magnetization M and $\overline{\dots}$ indicates the spatial average (i.e., the average over j). This expression indicates that the magnetostriction $\epsilon = \Delta L/L$ is a useful probe to detect local spin correlations $\langle \mathbf{S}_j \cdot \mathbf{S}_{j+n} \rangle_M$, although there are unknown coefficients f_n . For the sake of simplicity, we have neglected the contribution of the interchain coupling J_5 ; by including it, the change in the local spin correlation on the J_5 bond will be added to Eq. (2) with a coefficient $2f_5/k'$.

As Eq. (2) is similar to the expression of the spin-interaction energy E_{int} (i.e., the expectation value of the Heisenberg interaction part of the Hamiltonian), it is interesting to compare E_{int} with the measured $\Delta L/L$. Exploiting the thermodynamic relation $\frac{\partial E_{int}}{\partial M} = H$, the spin-interaction energy relative to the zero-field case can be obtained from the magnetization data (M vs H) via

$$\Delta E_{int}(M) \equiv E_{int}(M) - E_{int}(0) = \int_0^M H(M') dM'. \quad (3)$$

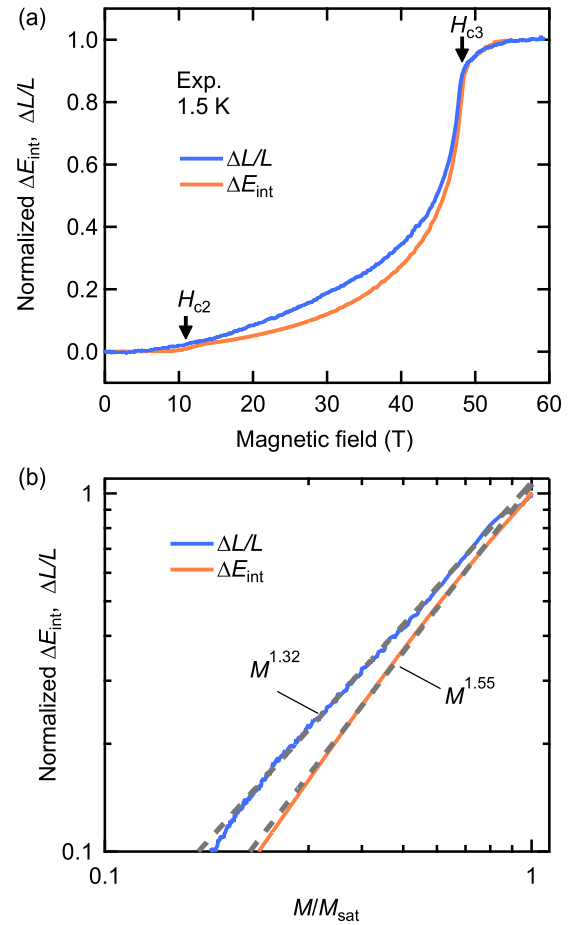


FIG. 3. (a) Magnetostriction $\Delta L/L$ and the spin-interaction energy ΔE_{int} of LiCuVO₄ at 1.5 K vs magnetic field. Both quantities are normalized to 1 at saturation. The spin-interaction energy is obtained from the magnetization reported in Ref. [28] through relation (3). (b) Logarithmic plot of $\Delta L/L$ and ΔE_{int} vs M . Dashed lines show power-law fits $\propto M^p$ with $p = 1.32$ for $\Delta L/L$ and $p = 1.55$ for ΔE_{int} (fit range is $0.4 \leq M/M_{sat} \leq 0.7$).

$\Delta L/L$ and ΔE_{int} are shown in Fig. 3, where both quantities are normalized to 1 at saturation. As seen in Fig. 3(a), the two curves exhibit an overall similar field dependence. A small deviation is found in the intermediate SDW phase between H_{c2} and H_{c3} . This indicates that the exchange-striction model, Eqs. (1) and (2), is a good approximation to describe the magnetoelastic properties of LiCuVO₄. We note that both $\Delta L/L$ and ΔE_{int} show a kink around H_{c3} ; the kink in ΔE_{int} is consistent with the theoretical picture of Ref. [25].

To analyze further the slightly different behavior of $\Delta L/L$ and ΔE_{int} , we plot them as a function of M/M_{sat} in logarithmic scales in Fig. 3(b). Our motivation for this plot stems from the fact that the power-law relation $\Delta L/L \propto M^p$ has been observed in a variety of magnetic materials: with $p = 2$ in conventional antiferromagnets, $p = 1$ in spin-dimer systems [37,38], and $p = 1.3$ in the distorted kagome-lattice magnet volborthite, Cu₃V₂O₇(OH)₂ · 2H₂O [36]. Here, $p = 2$ can be understood from a classical canted antiferromagnetic order, in which $\mathbf{S}_i = S(\sin \theta \cos \mathbf{q} \cdot \mathbf{r}_i, \sin \theta \sin \mathbf{q} \cdot \mathbf{r}_i, \cos \theta)$, with θ and \mathbf{q} being the canting angle and the propagation vector,

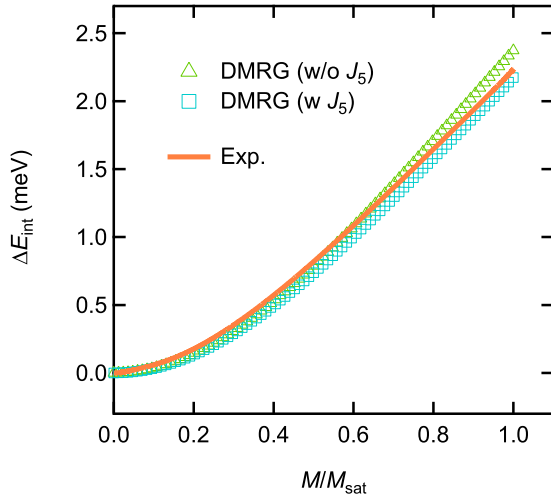


FIG. 4. Comparison of the spin-interaction energy ΔE_{int} per spin extracted from the experimental data with the DMRG results with and without the interchain coupling J_5 .

respectively. This gives

$$\begin{aligned} \mathbf{S}_i \cdot \mathbf{S}_j &= S^2 (\sin^2 \theta \cos \mathbf{q} \cdot \mathbf{r}_{ij} + \cos^2 \theta) \\ &= (S^2 - m^2) \cos \mathbf{q} \cdot \mathbf{r}_{ij} + m^2, \end{aligned} \quad (4)$$

with $m = S_i^z = S \cos \theta$ and $\mathbf{r}_{ij} = \mathbf{r}_i - \mathbf{r}_j$. $p = 1$ in spin-dimer systems is also comprehensible from the fact that the magnetization M and the change in the intradimer correlations $\langle \mathbf{S}_i \cdot \mathbf{S}_j \rangle_M$ are both proportional to the number of triplons. The unusual power $p = 1.3$ in volborthite could thus be interpreted as a result of strong quantum fluctuations in a low-dimensional frustrated magnet. As shown in Fig. 3(b), our data fit well to the relations $\Delta L/L \propto M^{1.32}$ and $\Delta E_{\text{int}} \propto M^{1.55}$ in the SDW phase. We will use these power-law relations as a guide to compare the experimental and numerical results. The exponents $p = 1.32$ and 1.55 are significantly different from that of conventional antiferromagnets; the former agrees with that for volborthite. This indicates a crucial role of quantum fluctuations in LiCuVO_4 due to its quasi-1D nature.

B. Comparison with numerical results

In Fig. 4, we compare the spin-interaction energy ΔE_{int} per spin extracted from the experimental data with the DMRG results with and without the interchain coupling J_5 . Here, the DMRG calculations were carried out for the pure 1D J_1 - J_2 model to obtain the spin-interaction energy without J_5 . The energy including J_5 was obtained in a mean-field manner, i.e., by simply adding $2J_5(M/2M_{\text{sat}})^2$ to the energy per spin of the pure 1D model [33]. The DMRG results modified by J_5 show a very good agreement with the experiment even without normalization for the vertical axis. The agreement is expected since ΔE_{int} is related to the magnetization via Eq. (3), and we have adjusted the value of J_2 in such a way that the DMRG result modified by J_5 can best reproduce the experimental magnetization (Appendix B).

In Fig. 5, we compare the experimental magnetostriction data with the DMRG results of the local spin correlations

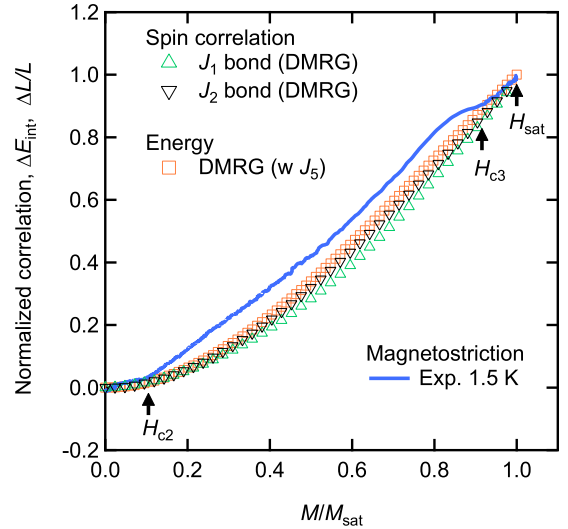


FIG. 5. Comparison of the magnetostriction results with the DMRG analyses on the local spin correlations $\langle \mathbf{S}_i \cdot \mathbf{S}_j \rangle_M - \langle \mathbf{S}_i \cdot \mathbf{S}_j \rangle_{M=0}$ on the J_1 and J_2 bonds and the spin-interaction energy ΔE_{int} . Here, all the quantities are normalized between 0 and 1, which correspond to the zero-field case and the saturation, respectively.

$\langle \mathbf{S}_i \cdot \mathbf{S}_j \rangle_M - \langle \mathbf{S}_i \cdot \mathbf{S}_j \rangle_{M=0}$ on the J_1 and J_2 bonds and the spin-interaction energy ΔE_{int} . Here, all the quantities are normalized between 0 and 1, which correspond to the zero-field case and the saturation, respectively. We calculated the local spin correlations in the finite chains with up to 168 spins and eliminated the finite-size and boundary effects from the data in order to obtain the estimates of $\langle \mathbf{S}_i \cdot \mathbf{S}_j \rangle_M$ on the J_1 and J_2 bonds in the thermodynamic limit. (See Appendix A for details of the analysis.) We also present the DMRG and ED results of the local spin correlations $\langle \mathbf{S}_i \cdot \mathbf{S}_j \rangle_M$ on the J_1 and J_2 bonds without normalization in Fig. 6.

Notably, in Fig. 5, the normalized spin correlations on the J_1 and J_2 bonds show quite similar behavior. This is remarkable as J_1 and J_2 are ferromagnetic and antiferromagnetic, respectively, and the correlations have opposite signs at low fields, as seen in Fig. 6. While we do not have a physical explanation for this behavior, it has the convenient consequence that any linear combination of the two local correlations shows similar behavior if normalized. Indeed, in Fig. 5, the DMRG data for the spin-interaction energy ΔE_{int} also behave similarly to the local spin correlations although it contains the small mean-field contribution of the interchain coupling J_5 . In contrast, the experimental magnetostriction data, $\Delta L/L$, which is also expected to be described by the local spin correlations on the J_1 and J_2 bonds according to Eq. (2), show a clear deviation in the SDW phase between H_{c2} and H_{c3} . This deviation cannot be explained even if we include a small contribution of the correlation on the J_5 bond, as we explain in the following. The calculated data in Fig. 6 are described well by the relation

$$\langle \mathbf{S}_i \cdot \mathbf{S}_j \rangle_M - \langle \mathbf{S}_i \cdot \mathbf{S}_j \rangle_{M=0} \propto M^p, \quad (5)$$

with $p = 1.82$, 1.74 , and 2 for the J_1 , J_2 , and J_5 bonds, respectively. Note that the relation with $p = 2$ for the J_5 bond is automatically satisfied in the mean-field treatment of J_5 ,

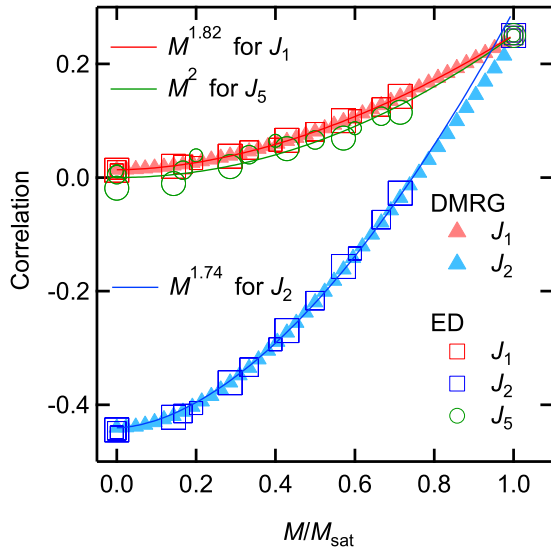


FIG. 6. Local spin correlations $\overline{\langle \mathbf{S}_i \cdot \mathbf{S}_j \rangle}_M$ on the J_1 , J_2 , and J_5 bonds calculated using DMRG and ED. Solid lines show the scaling [Eq. (5)] with $p = 1.82$, 1.74 , and 2 for the J_1 , J_2 , and J_5 bonds, respectively [39]. In the ED results, symbols with small, medium, and large sizes correspond to the cases of 20, 24, and 28 spins, respectively [screw boundary conditions [40] with $(L_x, L_y) = (5, 4)$, $(6, 4)$, and $(7, 4)$ as described in Appendix B].

and it is confirmed well in the ED result for the 2D model. A linear combination of the correlations (Fig. 6) cannot lead to the scaling of the magnetostriction $\Delta L/L \sim M^{1.32}$ in the SDW phase [Fig. 3(b)] as long as the contribution of the correlation on the J_5 bond is so small that the mean-field treatment is valid. Furthermore, such a linear combination cannot explain the kinklike features of the magnetostriction around the field-induced transition points H_{c2} and H_{c3} (Fig. 5).

The above consideration indicates a missing contribution in the magnetostriction. Such a contribution should be sensitive to the field-induced phase transitions as observed experimentally. A more refined treatment of the interchain coupling J_5 beyond the mean-field approximation might be required. It would also be important to investigate the effects of additional terms such as exchange anisotropy and DM interactions in the spin Hamiltonian and in the exchange-striction mechanism described by Eqs. (1) and (2).

IV. SUMMARY

We studied the magnetoelastic properties of the quasi-one-dimensional spin- $\frac{1}{2}$ frustrated magnet LiCuVO_4 using magnetostriction experiments and numerical analyses. Magnetostriction measurements of LiCuVO_4 in high magnetic fields up to 60 T applied along the b axis (1D spin-chain direction) show a monotonous increase of $\Delta L/L$ reaching a sizable value $\Delta L/L \approx 1.8 \times 10^{-4}$ at the saturation field $H_{\text{sat}} \approx 54$ T. Both the magnetostriction and the magnetization [28] evolve in a similar way between $H_{c3} \approx 48$ T and $H_{\text{sat}} \approx 54$ T, which indicates that both quantities consistently detect the 3D spin-nematic phase just below saturation. Our results were discussed within the exchange-striction mechanism. The DMRG and ED analyses on the local spin correlations and

spin-interaction energies for the J_1 - J_2 (- J_5) spin-chain model show a good agreement with the experimental observations. Small deviations found may indicate nontrivial changes in local correlations associated with field-induced phase transitions. A more refined treatment of the interchain coupling or additional interactions such as DM interactions would be needed to explain the magnetoelastic properties of LiCuVO_4 in more detail. As our results reveal the importance of the magnetoelastic coupling, it would be interesting to reconsider the contribution of the lattice to the multiferroic properties of LiCuVO_4 , which is under debate [15,30].

ACKNOWLEDGMENTS

We acknowledge support of the HLD at HZDR, member of the European Magnetic Field Laboratory (EMFL), the DFG through SFB 1143 and the Würzburg-Dresden Cluster of Excellence on Complexity and Topology in Quantum Matter–*ct.qmat* (EXC 2147, Project No. 390858490), and the BMBF via DAAD (Project No. 57457940). T.H. was supported by JSPS KAKENHI Grants No. JP17H02931 and No. JP19K03664. S.F. was supported by JSPS KAKENHI Grant No. JP18K03446.

APPENDIX A: DMRG CALCULATIONS

We performed DMRG calculations for the pure 1D J_1 - J_2 Heisenberg model with the Hamiltonian given by

$$\mathcal{H}_{\text{1D}} = J_1 \sum_j \mathbf{S}_j \cdot \mathbf{S}_{j+1} + J_2 \sum_j \mathbf{S}_j \cdot \mathbf{S}_{j+2}. \quad (\text{A1})$$

We set $J_1 : J_2 = -0.42 : 1$ as explained in Sec. II. The number of spins was up to $N_{\text{1D}} = 168$ and open boundary conditions were imposed.

Using DMRG, we calculated the lowest-energy state in each subspace characterized by the z component of the total spin, $S_{\text{tot}}^z = \sum_j S_j^z$. We then computed the lowest energy $E_{\text{int}}^{\text{1D}}(m)$ and the local spin correlations $\langle \mathbf{S}_j \cdot \mathbf{S}_{j+n} \rangle_m^{(0)}$ ($n = 1, 2$), where $m = S_{\text{tot}}^z / N_{\text{1D}}$ and $\langle \cdots \rangle_m^{(0)}$ denotes the expectation value with respect to the lowest-energy state in the subspace with $S_{\text{tot}}^z = N_{\text{1D}} m$ in the system under the open boundary conditions. Note that m relates to the magnetization M in the main text as $M = N g \mu_B m$, where N is the number of Cu^{2+} ions. The number of density matrix eigenstates kept in DMRG that is required for achieving a sufficient accuracy depends on N_{1D} and S_{tot}^z . In our calculation, we kept up to 600 states in the most severe case and the truncation error (the sum of the density matrix weights of discarded states averaged over the last sweep) was at most 6×10^{-7} . We thereby confirmed that the calculation was accurate enough for our argument.

The magnetization, which will be discussed in Appendix B, was obtained from the data of $E_{\text{int}}^{\text{1D}}(m)$ by finding m that minimizes $E_{\text{int}}^{\text{1D}}(m) - h N_{\text{1D}} m$ for each $h = g \mu_B H$. We found that S_{tot}^z appearing in the magnetization curve was all even except for the single case of $S_{\text{tot}}^z = 1$. This observation indicates the formation of bound magnon pairs for $S_{\text{tot}}^z \geq 2$. We note that this is consistent with the known result that the J_1 - J_2 Heisenberg chain with $J_1 < 0$, $J_2 > 0$, and $J_1/J_2 \gtrsim -1$ exhibits the Haldane dimer phase for $m = 0$

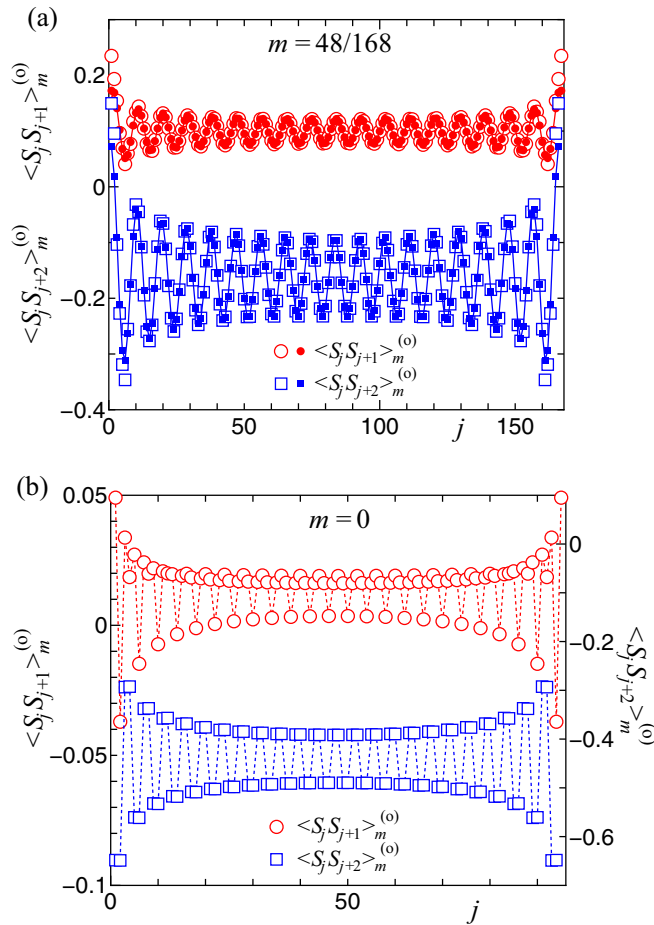


FIG. 7. (a) Local spin correlations $\langle \mathbf{S}_j \cdot \mathbf{S}_{j+n} \rangle_m^{(0)}$ ($n = 1, 2$) for $N_{\text{ID}} = 168$ and $m = 48/168$. Open and solid symbols respectively represent the DMRG data and fits using Eqs. (A2) and (A3). Solid lines connecting the fits are guides to the eye. (b) The DMRG data of $\langle \mathbf{S}_j \cdot \mathbf{S}_{j+n} \rangle_m^{(0)}$ for $m = 0$. The data for $N_{\text{ID}} = 96$ are shown to demonstrate oscillations with a four-site period. We observed similar four-site period oscillations also for $N_{\text{ID}} = 120$ and 168. Dashed lines connecting the data points are guides to the eye.

and the bimaggon TLL phase for $0 < m < 1/2$, while the range of the vector-chiral phase in between them, if any, is too narrow to be detected in the numerical calculation [2,3,41,42]. We consider only the states with even S_{tot}^z in the following analysis of the local spin correlations.

In Fig. 7, we present the DMRG data of the local spin correlations $\langle \mathbf{S}_j \cdot \mathbf{S}_{j+n} \rangle_m^{(0)}$ ($n = 1, 2$). Since the translational symmetry is broken by the open boundary conditions, the local spin correlations contain sizable contributions of boundary oscillation. We then found that, as shown in Fig. 7(a), the local spin correlations for $S_{\text{tot}}^z = N_{\text{ID}}m \geq 2$ were reproduced by the formulas

$$\langle \mathbf{S}_j \cdot \mathbf{S}_{j+1} \rangle_m^{(0)} = c_1 + c'_1 \frac{(-1)^j \cos [Q(j + 1/2)]}{[f(2j + 1)]^K}, \quad (\text{A2})$$

$$\langle \mathbf{S}_j \cdot \mathbf{S}_{j+2} \rangle_m^{(0)} = c_2 - c'_2 \frac{(-1)^j \sin [Q(j + 1)]}{[f(2j + 2)]^K}, \quad (\text{A3})$$

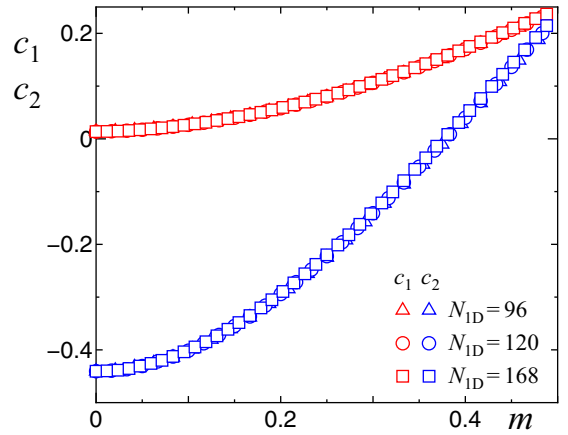


FIG. 8. Uniform parts of the local spin correlations, c_1 and c_2 , as functions of m . These were obtained from the fitting of the DMRG data of $\langle \mathbf{S}_j \cdot \mathbf{S}_{j+n} \rangle_m^{(0)}$ for $N_{\text{ID}} = 96, 120$, and 168 with Eqs. (A2) and (A3) as shown in Fig. 7(a).

with

$$f(x) = \frac{2(N_{\text{ID}} + 1)}{\pi} \sin \left(\frac{\pi |x|}{2(N_{\text{ID}} + 1)} \right), \quad (\text{A4})$$

that were derived as the expressions of the local energy density of the bimaggon TLL under open boundary conditions [2,43,44]. The wave number Q relates to m via the density of bimagnons ρ as

$$Q = \frac{2\pi N_{\text{ID}}}{N_{\text{ID}} + 1} \left(\rho - \frac{1}{2} \right), \quad (\text{A5})$$

$$\rho = \frac{1}{2} \left(\frac{1}{2} - m \right). \quad (\text{A6})$$

We performed the least-squares fitting of the DMRG data of $\langle \mathbf{S}_j \cdot \mathbf{S}_{j+n} \rangle_m^{(0)}$ ($n = 1, 2$) for $N_{\text{ID}}/4 + 1 \leq j \leq 3N_{\text{ID}}/4 - n$ with Eqs. (A2) and (A3) by taking c_n , c'_n , and K as fit parameters. We thereby determined the uniform parts of the correlations c_1 and c_2 and employed them as the estimates of the local spin correlations $\langle \mathbf{S}_i \cdot \mathbf{S}_j \rangle_M$ on the J_1 and J_2 bonds discussed in the main text [45].

For $S_{\text{tot}}^z = 0$, where the system is in the Haldane-dimer phase [42], the local spin correlations are not described by formulas (A2) and (A3). Instead, we found that the correlations oscillated with a four-site period as shown in Fig. 7(b). We hence took the average of the correlations at four bonds around the center of the chain as the estimates of the uniform parts of the correlations.

Figure 8 shows the uniform parts c_1 and c_2 of the local spin correlations for $N_{\text{ID}} = 96, 120, 168$ as functions of m . The data exhibit a smooth behavior and the dependence on the system size N_{ID} is negligibly small. We thus used the data of c_1 and c_2 for $N_{\text{ID}} = 168$ as the estimates of the local spin correlations $\langle \mathbf{S}_i \cdot \mathbf{S}_j \rangle_M$ on the J_1 and J_2 bonds in the thermodynamic limit.

APPENDIX B: MAGNETIZATION

The magnetization was calculated using the DMRG and ED methods for the J_1 - J_2 - J_5 spin-chain model with

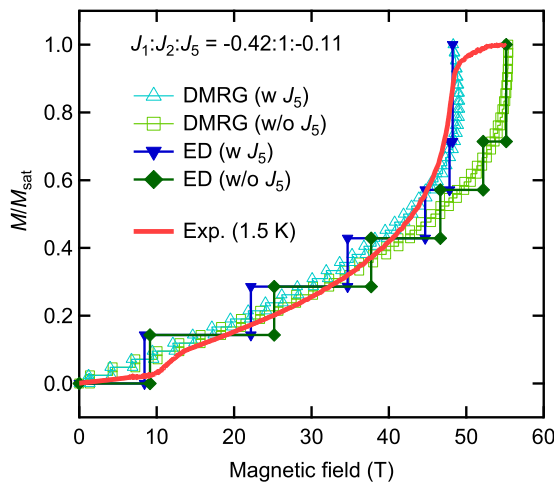


FIG. 9. Comparison of the magnetization data of LiCuVO₄ from Ref. [28] with the DMRG and ED results for the J_1 - J_2 - J_5 spin-chain model. Numerical results are presented for the cases with and without the interchain coupling J_5 to highlight its effect. In the DMRG result, J_5 is treated in a mean-field manner via a shift of the magnetic field by $4J_5(M/2M_{\text{sat}})/g\mu_B$ for each data point. For a ferromagnetic interchain coupling $J_5 < 0$, this treatment results in a small region near the saturation in which M/M_{sat} is multivalued, as seen in the figure; this should be regarded as an artifact of the mean-field treatment.

$J_1 : J_2 : J_5 = -0.42 : 1 : -0.11$, $J_2 = 4.0$ meV, and $g = 2.095$. The model can conveniently be defined on an approximate rectangular lattice with the primitive vectors $\mathbf{u} = (b/2, 0)$ and $\mathbf{v} = (0, a)$. The J_1 , J_2 , and J_5 interactions connect spins separated by the vectors \mathbf{u} , $2\mathbf{u}$, and $\pm\mathbf{u} + \mathbf{v}$, respectively. The DMRG calculations were performed for the pure 1D J_1 - J_2 model with $N_{1D} = 168$ spins, and the interchain coupling J_5 was taken into account in a mean-field manner [33]. Namely, at fixed $m = \frac{S_{\text{tot}}^z}{N_{1D}}$, the ground-state spin-interaction energy per spin $E_{\text{int}}^{1D}(m)/N_{1D}$ is modified by an additive correction of $2J_5m^2$. Correspondingly, in the magnetization (m vs $h = g\mu_B H = \frac{1}{N_{1D}} \frac{\partial E_{\text{int}}^{1D}(m)}{\partial m}$), h is modified by an additive correction of $4J_5m$. In contrast, the ED calculations were performed directly for the 2D model with 28 spins. To reduce the finite-size effects in ED, we adopted a screw boundary condition [40], in which spins separated by $L_x\mathbf{u} + \mathbf{v}$ and $L_y\mathbf{v}$ with $(L_x, L_y) = (7, 4)$ were identified.

In Fig. 9, the measured magnetization [28] and the DMRG and ED results are shown together. Here, the numerical results are presented for the cases with and without the interchain coupling J_5 to highlight its effect. We find a good agreement between the experimental data and the numerical results with J_5 coupling, which supports the present model. Furthermore, the agreement between the DMRG and ED results demonstrates the effectiveness of the mean-field treatment of J_5 in the DMRG calculations.

- [1] L. Kecke, T. Momoi, and A. Furusaki, *Phys. Rev. B* **76**, 060407(R) (2007).
- [2] T. Hikiyara, L. Kecke, T. Momoi, and A. Furusaki, *Phys. Rev. B* **78**, 144404 (2008).
- [3] J. Sudan, A. Lüscher, and A. M. Läuchli, *Phys. Rev. B* **80**, 140402(R) (2009).
- [4] L. Balents and O. A. Starykh, *Phys. Rev. Lett.* **116**, 177201 (2016).
- [5] A. Läuchli, G. Schmid, and S. Trebst, *Phys. Rev. B* **74**, 144426 (2006).
- [6] K. Harada, N. Kawashima, and M. Troyer, *J. Phys. Soc. Jpn.* **76**, 013703 (2006).
- [7] M. A. Lafontaine, M. Leblanc, and G. Ferey, *Acta Crystallogr., Sect. C* **45**, 1205 (1989).
- [8] A. V. Prokofiev, I. G. Vasilyeva, V. N. Ikorskii, V. V. Malakhov, I. P. Asanov, and W. Assmus, *J. Solid State Chem.* **177**, 3131 (2004).
- [9] M. Enderle, C. Mukherjee, B. Fåk, R. K. Kremer, J.-M. Broto, H. Rosner, S.-L. Drechsler, J. Richter, J. Malek, A. Prokofiev, W. Assmus, S. Pujol, J.-L. Raggazzoni, H. Rakoto, M. Rheinstädter, and H. M. Rønnow, *Europhys. Lett.* **70**, 237 (2005).
- [10] H.-J. Koo, C. Lee, M.-H. Whangbo, G. J. McIntyre, and R. K. Kremer, *Inorg. Chem.* **50**, 3582 (2011).
- [11] B. J. Gibson, R. K. Kremer, A. V. Prokofiev, W. Assmus, and G. J. McIntyre, *Physica B (Amsterdam)* **350**, E253 (2004).
- [12] M. Enderle, B. Fåk, H.-J. Mikeska, R. K. Kremer, A. Prokofiev, and W. Assmus, *Phys. Rev. Lett.* **104**, 237207 (2010).
- [13] Y. Naito, K. Sato, Y. Yasui, Y. Kobayashi, Y. Kobayashi, and M. Sato, *J. Phys. Soc. Jpn.* **76**, 023708 (2007).
- [14] F. Schrettle, S. Krohns, P. Lunkenheimer, J. Hemberger, N. Büttgen, H.-A. Krug von Nidda, A. V. Prokofiev, and A. Loidl, *Phys. Rev. B* **77**, 144101 (2008).
- [15] M. Mourigal, M. Enderle, R. K. Kremer, J. M. Law, and B. Fåk, *Phys. Rev. B* **83**, 100409(R) (2011).
- [16] A. Ruff, P. Lunkenheimer, H.-A. K. Krug von Nidda, S. Widmann, A. Prokofiev, L. Svistov, A. Loidl, and S. Krohns, *npj Quantum Mater.* **4**, 24 (2019).
- [17] N. Büttgen, W. Kraetschmer, L. E. Svistov, L. A. Prozorova, and A. Prokofiev, *Phys. Rev. B* **81**, 052403 (2010).
- [18] N. Büttgen, P. Kuhns, A. Prokofiev, A. P. Reyes, and L. E. Svistov, *Phys. Rev. B* **85**, 214421 (2012).
- [19] T. Masuda, M. Hagihala, Y. Kondoh, K. Kaneko, and N. Metoki, *J. Phys. Soc. Jpn.* **80**, 113705 (2011).
- [20] M. Sato, T. Hikiyara, and T. Momoi, *Phys. Rev. Lett.* **110**, 077206 (2013).
- [21] O. A. Starykh and L. Balents, *Phys. Rev. B* **89**, 104407 (2014).
- [22] M. Mourigal, M. Enderle, B. Fåk, R. K. Kremer, J. M. Law, A. Schneidewind, A. Hiess, and A. Prokofiev, *Phys. Rev. Lett.* **109**, 027203 (2012).
- [23] N. Büttgen, K. Nawa, T. Fujita, M. Hagiwara, P. Kuhns, A. Prokofiev, A. P. Reyes, L. E. Svistov, K. Yoshimura, and M. Takigawa, *Phys. Rev. B* **90**, 134401 (2014).
- [24] D. Hirobe, M. Sato, M. Hagihala, Y. Shiomi, T. Masuda, and E. Saitoh, *Phys. Rev. Lett.* **123**, 117202 (2019).
- [25] M. E. Zhitomirsky and H. Tsunetsugu, *Europhys. Lett.* **92**, 37001 (2010).
- [26] H. T. Ueda and K. Totsuka, *Phys. Rev. B* **80**, 014417 (2009).

- [27] L. E. Svistov, T. Fujita, H. Yamaguchi, S. Kimura, K. Omura, A. Prokofiev, A. I. Smirnov, Z. Honda, and M. Hagiwara, *JETP Lett.* **93**, 21 (2011).
- [28] A. Orlova, E. L. Green, J. M. Law, D. I. Gorbunov, G. Chanda, S. Krämer, M. Horvatić, R. K. Kremer, J. Wosnitza, and G. L. J. A. Rikken, *Phys. Rev. Lett.* **118**, 247201 (2017).
- [29] M. Gen, T. Nomura, D. I. Gorbunov, S. Yasin, P. T. Cong, C. Dong, Y. Kohama, E. L. Green, J. M. Law, M. S. Henriques, J. Wosnitza, A. A. Zvyagin, V. O. Chervanovskii, R. K. Kremer, and S. Zherlitsyn, *Phys. Rev. Research* **1**, 033065 (2019).
- [30] C. P. Grams, S. Kopatz, D. Brüning, S. Biesenka, P. Becker, L. Bohatý, T. Lorenz, and J. Hemberger, *Sci. Rep.* **9**, 4391 (2019).
- [31] R. Daou, F. Weickert, M. Nicklas, F. Steglich, A. Haase, and M. Doerr, *Rev. Sci. Instrum.* **81**, 033909 (2010).
- [32] H.-A. Krug von Nidda, L. E. Svistov, M. V. Eremin, R. M. Eremina, A. Loidl, V. Kataev, A. Validov, A. Prokofiev, and W. Abmus, *Phys. Rev. B* **65**, 134445 (2002).
- [33] O. A. Starykh, H. Katsura, and L. Balents, *Phys. Rev. B* **82**, 014421 (2010).
- [34] H. Nishimori, TITPACK version 2, http://www.qa.iir.titech.ac.jp/~nishimori/titpack2_new/index-e.html.
- [35] V. S. Zapf, V. F. Correa, P. Sengupta, C. D. Batista, M. Tsukamoto, N. Kawashima, P. Egan, C. Pantea, A. Migliori, J. B. Betts, M. Jaime, and A. Paduan-Filho, *Phys. Rev. B* **77**, 020404(R) (2008).
- [36] A. Ikeda, S. Furukawa, O. Janson, Y. H. Matsuda, S. Takeyama, T. Yajima, Z. Hiroi, and H. Ishikawa, *Phys. Rev. B* **99**, 140412(R) (2019).
- [37] M. Jaime, R. Daou, S. A. Crooker, F. Weickert, A. Uchida, A. E. Feiguin, C. D. Batista, H. A. Dabkowska, and B. D. Gaulin, *Proc. Natl. Acad. Sci. USA* **109**, 12404 (2012).
- [38] Y. Sawai, S. Kimura, T. Takeuchi, K. Kindo, and H. Tanaka, *Prog. Theor. Phys. Suppl.* **159**, 208 (2005).
- [39] The exponent p 's for the correlations on the J_1 and J_2 bonds were determined from the least-squares fitting of the DMRG data with Eq. (5) using the data for $0.4 \leq M/M_{\text{sat}} \leq 0.7$. On the other hand, the solid line for the correlations on the J_5 bond simply shows the relation $\overline{\langle \mathbf{S}_i \cdot \mathbf{S}_j \rangle_M} = (M/2M_{\text{sat}})^2$ expected in the mean-field treatment.
- [40] Y. Nishiyama, *Phys. Rev. B* **79**, 054425 (2009).
- [41] F. Heidrich-Meisner, I. P. McCulloch, and A. K. Kolezhuk, *Phys. Rev. B* **80**, 144417 (2009).
- [42] S. Furukawa, M. Sato, S. Onoda, and A. Furusaki, *Phys. Rev. B* **86**, 094417 (2012).
- [43] T. Hikiyara, A. Furusaki, and S. Lukyanov, *Phys. Rev. B* **96**, 134429 (2017).
- [44] T. Hikiyara and A. Furusaki, *Phys. Rev. B* **69**, 064427 (2004).
- [45] In fact, we found that the quality of the fitting became poor for small S_{tot}^z and near the saturation. Possible reasons for this include the following. First, the prediction of the bimagnon TLL theory is less accurate for small S_{tot}^z , where the one-magnon gap tends to be small, and also for S_{tot}^z close to the saturation, where the group velocity is small. Second, in deriving formulas (A2) and (A3), we neglected the effects of higher-order terms and the possible need to optimize the positions at which the Dirichlet boundary conditions are imposed (see, e.g., Ref. [43]). By simply applying formulas (A2) and (A3), we found that for those cases of S_{tot}^z the estimates of c'_n and K could not be obtained reliably as they were sensitive to the range of j used in fitting the data of $\langle \mathbf{S}_j \cdot \mathbf{S}_{j+n} \rangle_m^{(0)}$. However, even in such cases of S_{tot}^z , we could achieve robust estimates of the uniform part c_n , which were almost independent of the fitting range and expected to be reliable.